JOURNAL OF GEOPHYSICAL RESEARCH, VOL. 113, D02106, doi:10.1029/2007JD008568, 2008

Long-term memory in 1000-year simulated temperature records

Diego Rybski,[1] Armin Bunde,[1] and Hans von Storch[2]

Received 21 February 2007; revised 5 June 2007; accepted 16 August 2007; published 19 January 2008.

[1] We study the appearance of long-term persistence in temperature records, obtained from the global coupled general circulation model ECHO-G for two runs, using detrended fluctuation analysis. The first run is a historical simulation for the years 1000–1990 (with greenhouse gas, solar, and volcanic forcing), while the second run is a 1000-year "control run" with constant external forcings. We consider daily data of all grid points as well as their biannual averages in order to suppress 2-year oscillations appearing in the model records for some sites near the equator. Our results substantially confirm earlier studies of (considerably shorter) instrumental data and extend their results from decades to centuries. In the case of the historical simulation we find that most continental sites have correlation exponents γ between 0.8 and 0.6. For the ocean sites the long-term correlations seem to vanish at the equator and become nonstationary at the Arctic and Antarctic circles. In the control run the long-term correlations are less pronounced. Compared with the historical run, the correlation exponents are increased, and show a more pronounced latitude dependence, visible also at continental sites. When analyzing biannual averages, we find stronger long-term correlations in the historical run at continental sites and a less pronounced latitude dependence. In all cases, the exponent γ does not depend on the continentality of the sites.

Citation: Rybski, D., A. Bunde, and H. von Storch (2008), Long-term memory in 1000-year simulated temperature records, *J. Geophys. Res.*, *113*, D02106, doi:10.1029/2007JD008568.

1. Introduction

[2] In the past decade it has been recognized that multidecadal temperature records are long-term correlated [*Koscielny-Bunde et al.*, 1996; *Pelletier and Turcotte*, 1997; *Koscielny-Bunde et al.*, 1998; *Talkner and Weber*, 2000; *Weber and Talkner*, 2001; *Eichner et al.*, 2003; *Monetti et al.*, 2003; *Király et al.*, 2006], with a correlation exponent $\gamma \simeq 0.7$ for continental and coastline regions, and γ in a broad range around 0.4 for marine regions.

[3] The expressions "long-term correlated," "long-term persistent" or "long-term memory" refer to time series, whose autocorrelation functions do not decay exponentially, as is the case with autoregressive processes, but decay much slower following a power law. It has been suggested that the narrow spatial distribution of the exponent γ at continental and coastline stations may be used as an efficient test for the quality of climate models [*Govindan et al.*, 2002]. Newer analysis [*Vyushin et al.*, 2004] has revealed that climate simulations taking into proper account the natural forcings and in particular the volcanic forcings, reflect quite well this quite "universal" feature of the observable data.

[4] In this study, we extend these previous studies, which were restricted to simulated or observational data with a time span of not more than 200 years. We consider two 1000-year simulations, which have been carried out with the ECHO-G model, and hope that by this we can learn more about the persistence at larger timescales. In the first simulation, one considers historical conditions by applying variations in the greenhouse gas concentrations and in the solar activity, whereby the influence of volcanic activity is included in an effective solar constant [*Zorita et al.*, 2005]. In contrast, in the second simulation called "control run," no variations of external forcings are taken into account [*Zorita et al.*, 2003; see also *Fraedrich and Blender*, 2003].

[5] This article is organized as follows. In section 2, we give information of the climate model and the performed runs. In section 3, we describe the detrending analysis used in this paper, the DFA. In section 4, we present the results of this analysis. Section 5 concludes the paper with a discussion.

2. Description of Climate Model Simulations

[6] The climate model we consider is the global coupled general circulation model ECHO-G [*Legutke and Voss*, 1999]. The model consists of the atmosphere model ECHAM4 [*Roeckner et al.*, 1996] with a T30 resolution and 19 vertical levels (grid resolution approx. $3.75° \times 3.75°$) and the ocean model HOPE-G [*Wolff et al.*, 1997] with a grid resolution of $2.81° \times 2.81°$ and 20 vertical

[1] Institut für Theoretische Physik III, Universität Giessen, Giessen, Germany.
[2] Institute for Coastal Research, GKSS Research Centre, Geesthacht, Germany.

0148-0227/08/2007JD008568$09.00

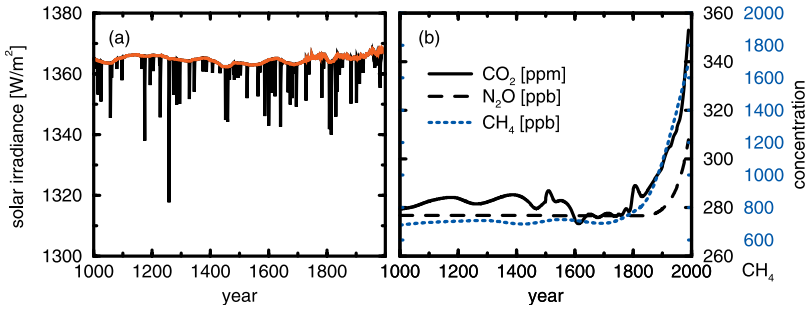

Figure 1. Forcings applied to the historical simulation with the global coupled general circulation model ECHAM4/HOPE-G. (a) Variations in the solar constant (red line) and the effective solar constant (black), which takes into account a reduction caused by volcanic aerosols. Note the small absolute variations of this quantity. (b) Variations of the considered greenhouse gas concentrations, namely CO_2, CH_4 and N_2O.

levels. An increased tropical resolution, reaching a mesh size of 0.5 at the equator, was implemented to allow for a better representation of equatorial dynamics. Constant, zero-average flux correction of heat and freshwater is applied in order to avoid climate drift in such a long simulation.

[7] One run operates with constant driving factors, i.e., solar insolation (with an annual cycle), as well as aerosol and greenhouse gas load [*Zorita et al.*, 2003]. The other one is a historical simulation [*Zorita et al.*, 2005] for the period 1000–1990 A.D. (991 years), which was forced with reconstructions of solar [*Lean et al.*, 1995], volcanic activity [*Crowley*, 2000], and greenhouse gas concentrations [*Etheridge et al.*, 1996] during the last millennium (Figure 1). The solar constant was scaled to a difference between the Late Maunder Minimum and present day of 0.3%. This historical simulation does neither consider changes in anthropogenic atmospheric aerosol concentrations nor changes in the vegetation cover or land use. Here we analyze the near-surface temperature records (measured 2 m above the surface) of all 4608 grid points for both runs.

3. Long-Term Memory and Detrended Fluctuation Analysis

[8] Consider a record T_i, where the index i counts the days in the record, $i = 1, 2, \ldots, N$. The T_i represent the daily temperature, measured at a certain meteorological station or grid point. For eliminating the periodic seasonal trends, we concentrate on the departures of T_i,

$$\tau_i = T_i - \overline{T}_i \ . \tag{1}$$

from their mean daily value $\overline{T}_i$ for each calendar date i, say, 2 March, which has been obtained by averaging over all years in the record.

[9] To quantify long-term persistence (long-term correlations) we consider the (auto-) correlation function between two τ_i values separated by s days,

$$C(s) \equiv \frac{\langle \tau_i \tau_{i+s} \rangle}{\langle \tau_i^2 \rangle} = \frac{1}{(N-s)\langle \tau_i^2 \rangle} \sum_{i=1}^{N-s} \tau_i \tau_{i+s} \ . \tag{2}$$

If the τ_i are uncorrelated, $C(s)$ is zero for s positive. If correlations exist up to a certain number of days $s_\times$, the correlation function will be positive up to $s_\times$ and vanish above $s_\times$. For the relevant case of long-term correlations, the correlation function decays with a power law,

$$C(s) \sim s^{-\gamma}, \quad 0 < \gamma < 1 \ . \tag{3}$$

A correct evaluation of $C(s)$ is difficult for large s where $C(s)$ reaches small values and fluctuates around zero. Furthermore nonstationarities in the data will lead to incorrect estimations of correlations.

[10] Therefore, to identify long-term correlations on large scales s we do not calculate $C(s)$ directly, but instead study the "profile"

$$Y_m = \sum_{i=1}^{m} \tau_i \ . \tag{4}$$

The fluctuations of the profile, in a window of size s, are related to the correlation function $C(s)$. In the case of long-term power law correlations, equation (3), the mean fluctuations $F(s)$, obtained by averaging over many time windows of size s (see below) scale as [see, e.g., *Bunde et al.*, 2002]

$$F(s) \sim s^{\alpha}, \quad \alpha = 1 - \gamma/2 \ . \tag{5}$$

For uncorrelated data (as well as for correlations decaying faster than $1/s$), we have $\alpha = 1/2$.

[11] For the determination of the fluctuation function $F(s)$, we have employed several orders of the detrended fluctuation analysis (DFA). For a detailed description of the methods we refer to *Kantelhardt et al.* [2001].

[12] 1. In the zero-order detrended fluctuation analysis (DFA0) (where trends are not going to be eliminated), we determine in each window the mean value of the profile. The variance of the profile from this constant value represents the square of the fluctuations in each window.

[13] 2. In the first-order detrended fluctuation analysis (DFA1), sometimes also called DFA [*Peng et al.*, 1994], we determine in each window the best linear fit of the profile. The variance of the profile from this straight line represents the square of the fluctuations in each window.

[14] 3. In general, in the nth-order DFA (DFAn) we determine in each window the best nth-order polynomial

fit of the profile [*Bunde et al.*, 2000]. The variance of the profile from these best nth-order polynomials represents the square of the fluctuations in each window.

[15] By definition, DFA0 does not eliminate trends, while DFAn eliminates trends of order n in the profile and $n - 1$ in the original time series. Thus, from the comparison of fluctuation functions $F(s)$ obtained from different methods, one can learn about both long-term correlations and the influence of trends [*Kantelhardt et al.*, 2001] (see also D. Rybski and A. Bunde, Trends in long-term correlated records: Detection using DFA, preprint, 2008).

[16] We would like to note that DFA0 is equivalent to the simplest fluctuation analysis (FA) [*Koscielny-Bunde et al.*, 1998] which is identical to the aggregated standard deviation method (ASD) [see, e.g., *Koutsoyiannis*, 2006].

[17] The accuracy of $F(s)$ decreases with increasing window size. It is usually assumed that s should not be larger than one quarter of the record length in order to guarantee a reasonable statistics.

4. Analysis of Temperature Records

[18] To check for long-term correlations, we first applied DFA0-DFA3 to the daily data of both, historical simulation and control run, and calculated, for each of $96 \times 48 = 4608$ records obtained from each run of the model, the corresponding fluctuation functions. To obtain the exponent α, we fitted a power law to the fluctuation function in the time regime between approximately 2 and 200 years. Owing to the large amount of data, we could not check the quality of the fit for all records. In some cases, as we will show below, semistable oscillations occur in the fluctuation functions. Consequently, there is no scaling and a power law fit is not meaningful. If it is nevertheless done, it leads to incorrect results for the scaling exponents α and γ. Even an automated evaluation of the squared deviations between $F(s)$ and its power law fit does not work, since oscillations in $F(s)$ lead to spurious straight lines in a double-logarithmic presentation on large scales, as is shown below.

[19] In some areas, in particular in the equatorial Pacific, biannual cycles occur, a feature at variance with observational evidence. Unfortunately, these cycles cannot be eliminated simply by a seasonal detrending analog to equation (1), since the period of 2 years is too unstable. For the same reason, we were not able to remove the oscillations (automatically) in the Fourier spectrum. Therefore, in order to get rid of these oscillations, we additionally consider time series of biannual temperatures (i.e., temperature averaged over 2 years of daily data). With this renormalization (aggregation) we also verify that scaling in the daily data is not due to a short-term process with a correlation length below 2 years. The disadvantage of considering biannual data is that the number of data points is reduced by a factor 720 compared with the daily data.

[20] Figure 2 shows the results for the fluctuation exponents obtained by DFA2 for the historical simulation (Figures 2a and 2b) and the control run (Figures 2c and 2d), for daily data and for the biannual data. Note that in the Cartesian projection, the areas of the grid points are overestimated at the poles and underestimated at the equator. Values of α below 0.475 (white) and above 1.025 (black) are not discriminated, since we are only interested in stationary long-term correlated data ($0.5 < \alpha < 1.0$). Values of α between 0.475 and 0.525 indicate white noise behavior and are in violet, while α values between 0.975 and 1.025, which indicate $1/f$ noise, are in red.

[21] When analyzing the daily data of the historical simulation (Figure 2a) we find large violet and white areas where $\alpha \leq 0.5$ close to the equator, and red and black areas where $\alpha \geq 1.0$ close to the Antarctica and Greenland. These findings will be discussed separately below.

[22] In general, over land mainly exponents between 0.6 and 0.7 occur for daily data. For Europe, where the longest instrumental records are available, the α values of about 0.65 derived from observed temperature series [*Koscielny-Bunde et al.*, 1998] are well reproduced. Over the oceans, the long-term correlations are more pronounced. For the northern part of the Pacific and the Atlantic Ocean mainly exponents between 0.7 and 0.85 are found. There is a weak latitude dependence of α, which on the average close to the equator is lower than close to the Arctic and Antarctic circles. This dependence is more pronounced for the control run (see Figure 2c). When α is obtained from the biannual data sets, on the other hand, the latitude dependence of α is much less pronounced (Figure 2d). In Figure 2a also some ocean currents can be identified, like the Kuroshio current close to Japan with increased values of α (orange) or the South Equatorial current, best visible in the Indian Ocean, with lower values of α (blue-violet). In the biannual data, Figures 2b and 2d, the differences between ocean and continental sites are less pronounced and the fluctuation exponents at continental sites are larger.

[23] We would like to note that the solar activity (Figure 1) itself exhibits nonstationary random-walk-like behavior, while the effective solar constant shows long-term correlations with an asymptotic fluctuation exponent of approximately 0.9. For the control run, the fluctuation exponents are considerably smaller than for the historical simulation: The areas with $\alpha \leq 0.5$ (white) or $\alpha \geq 1.0$ (black) are larger. Also, at grid points far from the oceans the correlations are weaker than for the historical simulation. This indicates that the forcings of the historical simulation represent important contributions to the strength of the long-term correlations of the near-surface temperature [see also *Vyushin et al.*, 2004].

[24] Figures 3–6 show, on the right-hand side, examples of fluctuation functions of the historical simulation (circles), of the control run (squares) and, if available of instrumental (asterisk) or reconstructed (plus) records. We also show, for comparison, the fluctuation functions of the biannual temperature data of the historical simulation (filled circles). In the case of the historical simulation, the fluctuation functions of DFA0 and DFA1 are affected by trends, whereas DFA of higher order ($n \geq 2$) exhibit similar fluctuation functions. Thus, to compare the results of both simulations, we show only the DFA2 fluctuation functions. For illustration, on the left-hand side of Figures 3–6, 10 years of the deseasoned temperature records from the historical simulation are also shown, and, if available, parts of the corresponding deseasoned instrumental record. The time series derived from instrumental observations show somewhat larger variability than the historical simulation, since the former represent point observations whereas the model data represent grid box averages, across about 300 km by 300 km.

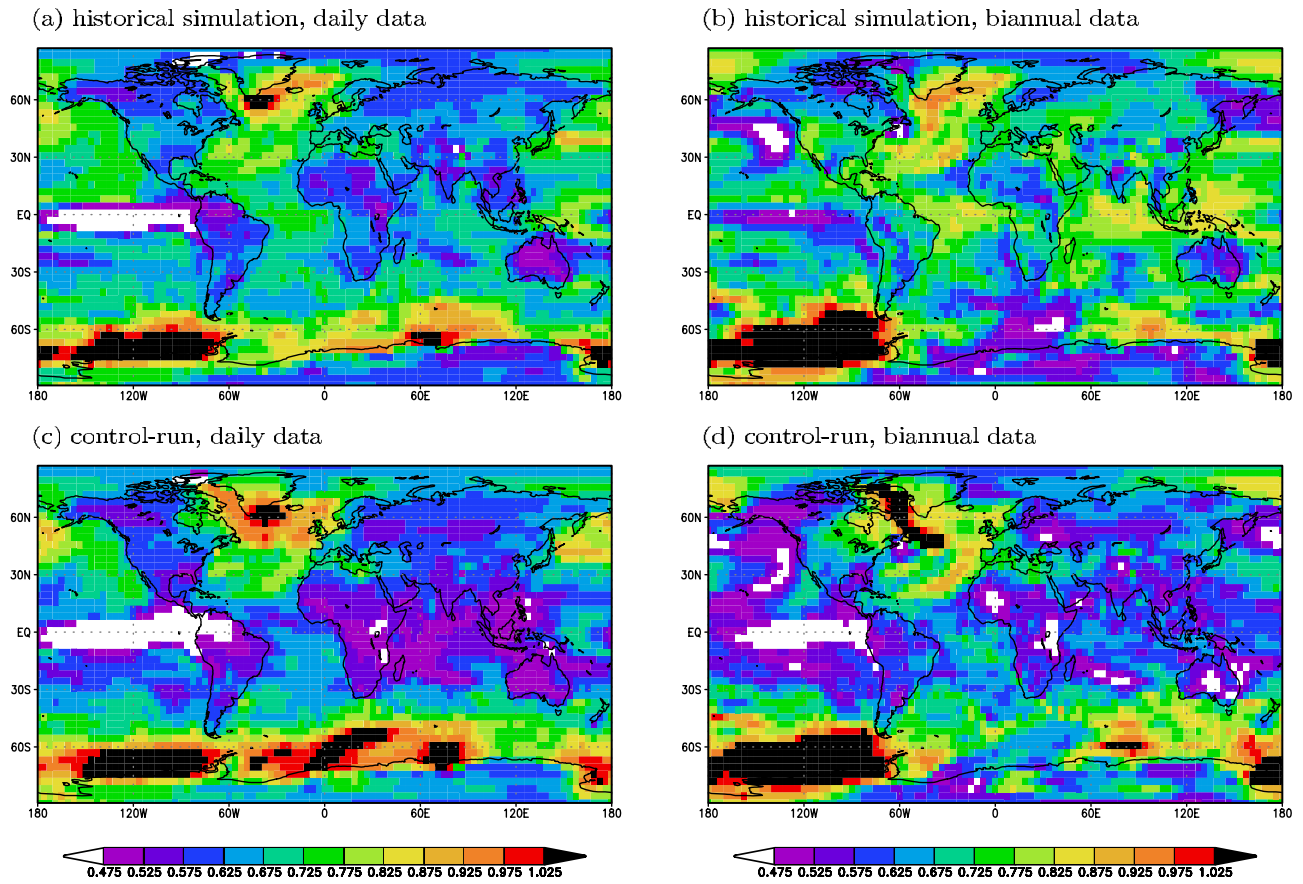

Figure 2. Global distribution of DFA2 fluctuation exponents calculated for the 2-m-temperature records (a, b) of the historical simulation integrated from 1000 to 1990 and (c, d) of the 1000-year control run. Figures 2a and 2c are daily records, and the fluctuation exponents α were determined on scales between 850 and 70000 days. Figures 2b and 2d are biannual records, and the fluctuation exponents α were determined on scales between 6480 and 80000 days.

[25] Figures 3 and 4 present examples for the vast majority of fluctuation functions that show, apart from a crossover at short timescales, excellent scaling behavior. In Figure 3, continental grid points close to the meteorological stations of Chita, Prague, and Albany are treated. In the double-logarithmic presentation, the fluctuation functions for instrumental (upper curves) and simulated records are straight lines for large scales [*Eichner et al.*, 2003], with slopes α close to 0.65 for the instrumental and the simulated historical records. Accordingly, the historical simulation reproduces remarkably well the long-term persistence of near-surface temperatures at most sites, while the control run underestimates the long-term persistence. The left-hand side of Figure 3 shows that after deseasoning, the data still show a seasonal trend in the standard deviation of the temperature. This seasonal trend is slightly exaggerated in the model simulation. However, since the DFA is not sensitive to these nonstationarities [*Chen et al.*, 2002], the exponents remain unchanged.

[26] Since the temperature anomalies of both, model and real data, are roughly normal distributed and their probability distributions do not show a fat tail, we conclude that the fluctuation exponents $\alpha > 0.5$ are due to long-term correlations and not due to a broad probability distribution of the temperature anomalies (Joseph phenomenon versus Noah phenomenon [see *Mandelbrot and Wallis*, 1968]). This is further verified by a separate analysis, where we eliminated the correlations by randomly shuffling the τ_i. This shuffling has no effect on the probability distribution function of τ_i. We find that the exponent α characterizing the fluctuations in the shuffled records is 1/2, indicating that the Joseph phenomenon is the main effect.

[27] In Figure 4 a typical site in the Northern Atlantic is considered. For this site the exponent α of the fluctuation function is around 0.74 for the daily data and around 0.79 for the biannual data. Both results are in substantial agreement with the analysis of the data obtained by *Kaplan et al.* [1998], which yields $\alpha \simeq 0.84$ [see also *Monetti et al.*, 2003]. While the vast majority of data exhibits excellent scaling, there are several regions where scaling is not so good, in particular close to the sea ice margin near Greenland and the Antarctica, and in areas affected by El Niño Southern Oscillation (ENSO).

[28] Figure 5 shows both daily temperature fluctuations around the seasonal mean and the fluctuation functions, for sites located close to Greenland (Figures 5a and 5b) and Antarctica (Figures 5c and 5d). In the double-logarithmic presentation, the fluctuation functions do not follow straight lines and therefore the automatic fitting procedure for the determination of α is meaningless. In both model runs,

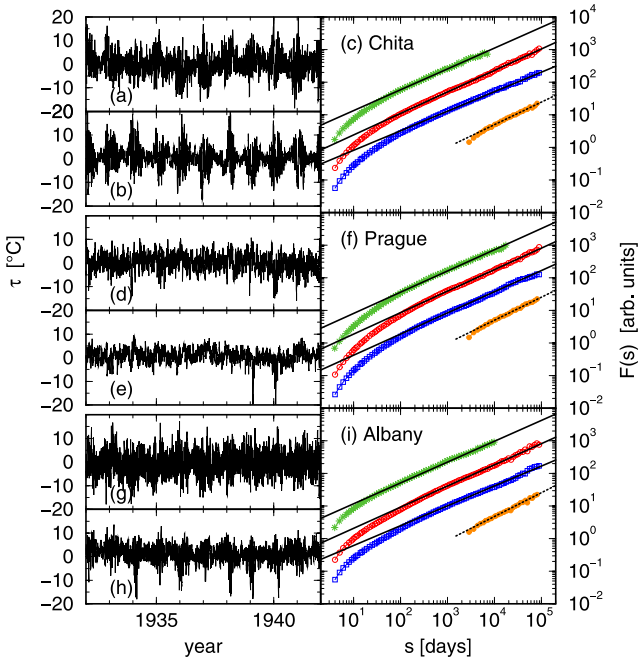

Figure 3. Daily temperature fluctuations around the seasonal cycle and DFA2 fluctuation functions for three continental grid points on the globe. (a–c) Chita (112.50E, 53.81N), (d–f) Prague (15.00E, 50.10N), and (g–i) Albany (−75.00E, 42.68N). Figures 3a, 3d, and 3g are instrumental records, and Figures 3b, 3e, and 3h are historical simulations. Figures 3c, 3f, and 3i show the fluctuation functions $F(s)$ versus timescale s for the instrumental record (asterisk, upper curve), for the historical simulation (open circles), for the control run (open squares), and for the biannual values of the historical simulation (solid circles, lower curve). The grid points of the model data were chosen nearest to the meteorological stations. The straight lines in Figures 3c, 3f, and 3i have the slopes (from top to bottom): 0.64, 0.66, 0.60, and 0.69 (Figure 3c); 0.65, 0.66, 0.65, and 0.71 (Figure 3f); and 0.64, 0.65, 0.61, and 0.73 (Figure 3i).

humps occur in the curves, which are caused by strong oscillations in the records. These oscillations are visible in Figures 5a and 5c and are leftovers of the seasonal trend after the deseasoning, probably due to very large interannual fluctuations. It is well known that DFA is sensitive to oscillations in the mean of the records [*Kantelhardt et al.*, 2001]: On scales below the period (360 days in the model), the oscillations yield strong correlations, leading to large exponents in the fluctuation functions, while on scales above the period, the oscillations induce anticorrelations, with smaller fluctuation exponents. Thus oscillations hide the true scaling and lead to an overestimation of α on short timescales and an underestimation on larger timescales. By definition, to exclude biannual oscillations, one needs a sample rate of at most 2 years. Figure 5 shows, that also the biannual data on large scales are characterized by an exponent α above 1, i.e., show nonstationary behavior. Unfortunately there are no long instrumental records for these regions that can be compared with the model results. We cannot exclude that this nonstationarity is an artifact of the model.

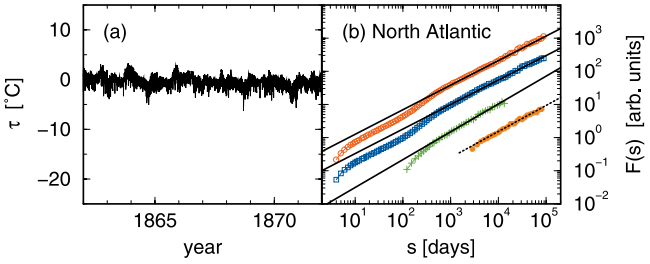

Figure 4. Daily temperature fluctuations around the seasonal cycle and DFA2 fluctuation functions for a grid point in the North Atlantic (−150.00E, 42.68N). (a) Ten years of the deseasoned daily data of the historical simulation. (b) Fluctuation functions $F(s)$ versus timescale s for the historical simulation (open circles, upper curve), for the control run (open squares), for the sea surface temperature (pluses) [*Kaplan et al.*, 1998], and for the biannual values of the historical simulation (solid circles, lower curve). Since the sea surface temperature estimated by *Kaplan et al.* [1998] has monthly resolution, the s values start at 4 × 30 days. In Figure 4b we find the slopes (from

[29] Next we discuss the areas under the influence of ENSO, which are the west coast of Southern America and the complete equatorial Pacific regime. Exceptionally warm (El Niño) and cold (La Niña) sea surface temperatures occur irregularly on a timescale of 3–8 years [*Glantz*, 2000], while the model generates an almost periodic behavior with a periodicity of 2 years. The grid points we inspect are located in central Africa (Figures 6a and 6b), in the Pacific on the

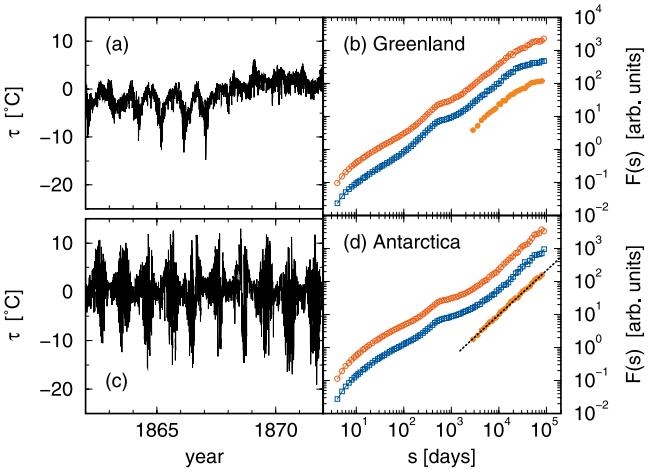

Figure 5. Daily temperature fluctuations around the seasonal trend (historical simulation) and DFA2 fluctuation functions for two grid points close to the sea ice margin. (a, b) Close to Greenland (−41.25E, 57.52N) and (c, d) close to Antarctica (−142.50E, −72.36N). Figures 5b and 5d show the fluctuation functions $F(s)$ versus timescale s for the historical simulation (open circles, upper curve), for the control run (open squares, central curve), and for the biannual values of the historical simulation (solid circles, lower curve). The dashed line in Figure 5d has the slope

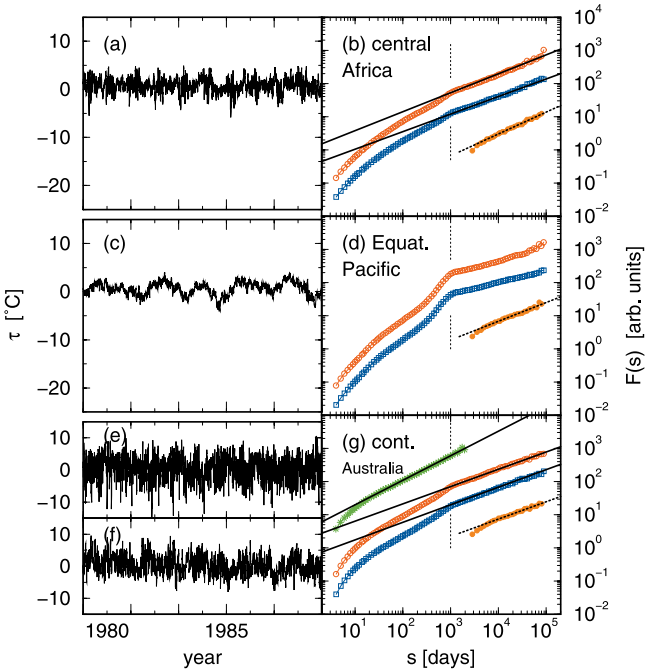

Figure 6. Daily temperature fluctuations around the seasonal cycle and DFA2 fluctuation functions for three grid points under the influence of ENSO. (a, b) Central Africa (26.25E, 5.57N), (c, d) equatorial Pacific (−93.75E, −1.86N), and (e−g) continental Australia (146.25E, −27.83N). Figure 6e shows part of the deseasoned instrumental temperature record of Charleville (AUS), while Figure 6f shows the corresponding data from the historical simulation for the nearest grid point. Figures 6b, 6d, and 6g show the fluctuation functions $F(s)$ versus timescale s for the historical simulation (open circles, upper curve), for the control run (open squares, central curve), and for the biannual values of the historical simulation (solid circles, lower curve). In addition, the upper most curve in Figure 6g gives the fluctuation function for Charleville (1942−1999) in Australia (146.27E, −26.42N). The straight lines in Figures 6b, 6d, and 6g have the slopes (from top to bottom): 0.57, 0.53, and 0.66 (Figure 6b); 0.56 (Figure 6d); and 0.74, 0.52, 0.53, and 0.52 (Figure 6g). The dotted vertical lines indicate the timescale s = 1000. Crossovers appear in DFA on larger scales the larger the detrending order n is (1000 > 2 × 360) [*Kantelhardt et al.*, 2001].

latitude of the equator (Figures 6c and 6d), and in central Australia (Figures 6e−6g).

[30] For the African temperature records (Figure 6a), the fluctuation functions (Figure 6b) exhibit a hump, which here is not located at a period of 1 year like in Figure 5, but at a period of about 2 years. Again, the remaining oscillations in the deseasoned data lead to a larger slope in $F(s)$ below 2 years and to a smaller slope above 2 years. A linear fit between 2 and 200 years will thus lead to exponents around 0.5 and to the misleading conclusion that the data are asymptotically like white noise.

[31] This effect is even stronger in the equatorial Pacific, where the simulations exhibit exponents α considerably smaller than 0.5, seeming to suggest the presence of long-term anticorrelations in ENSO areas. However, this is certainly an artifact as the real underlying temporal correlation structure is masked by the (irregularly occurring) ENSO. Since there are no long instrumental data in Central Africa and the equatorial Pacific, we cannot decide, how much the model exaggerates the influence of ENSO. However, the fluctuation functions for the biannual data, Figures 6b, 6d and 6g) (bottom curves), show exponents α slightly above 0.5.

[32] Instrumental data exists for central Australia. Figure 6e shows part of the temperature record of Charleville in continental Australia and Figure 6f shows the corresponding historical simulation temperatures. Again we find small humps in the fluctuation functions of the model runs (Figure 6g). In the simulation, possibly the influence of the insufficiently modeled ENSO leads to smaller slopes also here, since in the temperature record of the historical simulation a pattern of 2 years can be found (Figure 6f). As Figure 6e shows, these strong oscillations do not exist in the instrumental record. The fluctuation function yields an exponent $\alpha \simeq 0.74$ (on scales $40 < s < 2000$ days), characteristic of strong long-term correlations, while the simulation records, for both daily and biannual data, are described by $\alpha \simeq 0.5$ (on scales $850 < s < 70000$).

[33] Our results are summarized in Figure 7 and Table 1. In order to better assess the fluctuation exponents presented in Figure 2, we averaged them along the circles of latitude separately for land and ocean grid points. In Figure 7 the average values and standard deviations are plotted against the latitude. Figures 7a−7d show the values for daily data, while Figures 7e−7h give the values for biannual data. This representation has to be regarded with care, since on one hand the values come with large uncertainty (partial systematically) and on the other hand geographical regions are not being distinguished. For the historical simulation and daily data, the average fluctuation exponents for latitudes over land (Figure 7a) are rather inside to expected range $0.6 < \alpha < 0.7$, although near-equator latitudes exhibit weakly reduced average α. For oceans (Figure 7c) a pronounced latitude dependence is found, as described above. This dependence (v shape) is more distinct in the case of the control run (Figures 7b and 7d), where in general smaller average α are found. For biannual data (Figures 7e−7h) our analysis leads to a less pronounced systematic latitude dependence and especially for the historical simulation to overall larger average α. The larger standard deviations for biannual data are possibly due to the smaller fitting range of $F(s)$.

[34] In Table 1 we give areal averages of the obtained fluctuation exponents (both model runs, daily and biannual resolution) for the continents Eurasia, Africa, North America, and Australia. Again, the tendency of reduced exponents for the control run is supported. On the other hand, the areal averages for the biannual resolution are larger compared to those for daily resolution. The average values for Eurasia (0.67 ± 0.06) and America (0.66 ± 0.06) are in good agreement with results for instrumental data of other authors, although the standard deviations are rather large.

5. Discussion

[35] In this article we have considered near-surface air temperature records obtained from the global coupled

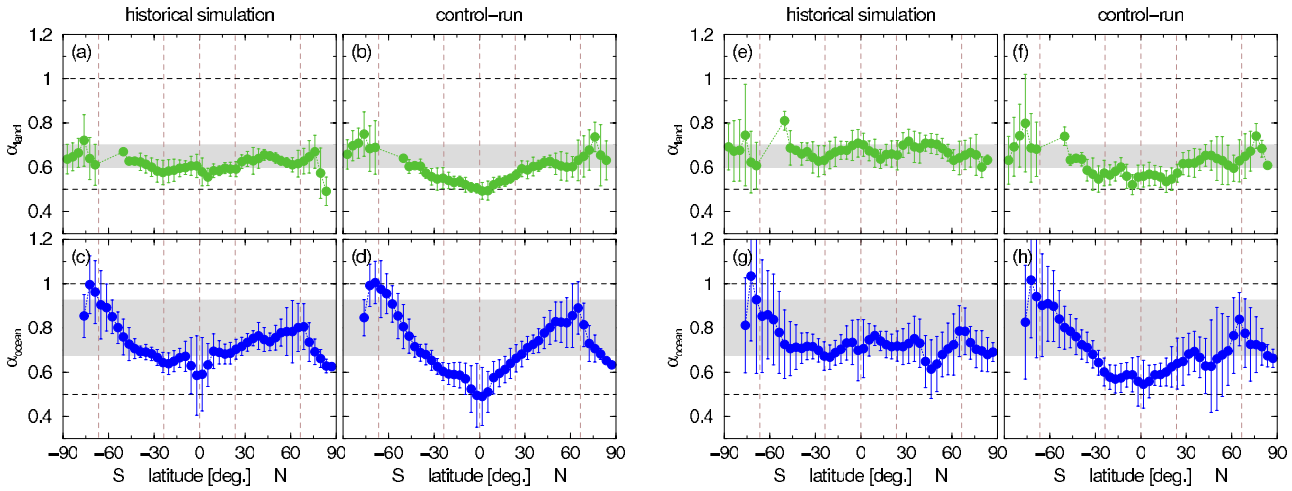

Figure 7. Values for the DFA2 fluctuation exponent averaged along the circles of latitude, separated into (top) land and (bottom) ocean grid points for (a–d) daily and (e–h) biannual data. In Figures 7a, 7c, 7e, and 7g we consider the historical simulation, and in Figures 7b, 7d, 7f, and 7h we consider the control run. The plots show the average fluctuation exponents with the standard deviations as error bars against the geographical latitude (south: left, north: right). (a) Daily data, historical simulation, land; (b) daily data, control run, land; (c) daily data, historical simulation, ocean; (d) daily data, control run, ocean; (e) biannual data, historical simulation, land; (f) biannual data, control run, land; (g) biannual data, historical simulation, ocean; and (h) biannual data, control run, ocean. The grey areas indicate the range of exponents found in instrumental records, $0.6 < \alpha_{land} < 0.7$ for continental sites [*Eichner et al.*, 2003] and $0.675 < \alpha_{ocean} < 0.925$ for ocean sites [*Monetti et al.*, 2003]. The horizontal dashed lines indicate the uncorrelated case ($\alpha = 0.5$) and the border to nonstationarity ($\alpha = 1.0$). The vertical dashed lines represent the Arctic and Antarctic circles (±66.5°), the Tropic of Cancer or Capricorn (±23.5°), and the equator.

general circulation model ECHO-G in two runs, a historical simulation for the years 1000–1990 (with greenhouse gas, solar, and volcanic forcing) and a 1000-year control run. In order to quantify the long-term correlations, we have applied detrended fluctuation analysis to the records of all grid points, for both runs, and for daily as well as biannual resolution.

[36] In the case of the historical simulation we find that most continental sites have fluctuation exponents α between 0.6 and 0.7. Near the equator the exponents of the historical simulation seem to be smaller, which is possibly an artifact due to ENSO. For the ocean sites, the exponents depend on the latitude, with α around 0.5 at the equator and $\alpha \gtrsim 1$ at the Arctic and Antarctic circles. In the control run the fluctuation exponents are reduced, the latitude dependence is more pronounced and also visible at continental sites. We have also analyzed biannual data, where cycles with a period of up to 2 years are suppressed, and find stronger long-term correlations in the historical run at continental sites and a less pronounced latitude dependence.

[37] The exponents obtained for continental sites from the historical run are rather in agreement with the values found by *Eichner et al.* [2003], who report $\alpha \simeq 0.6 \ldots 0.7$ with a maximum at 0.65, and by *Király et al.* [2006], who find $\alpha \simeq 0.63 \ldots 0.75$ with a maximum at approximately 0.69. By studying the 1000-year record of the historic run we have found that these long-term correlations should hold at least for 200 years, considerably extending the largest scales for instrumental records of typically 50 years [see also *Rybski et al.*, 2006]. This outcome is rather surprising, since in a such long model run, which already is affected by accumulation of model error and difficulty in simulating long-term changes in ocean circulation, processes governing longer-term climate change, such as vegetation and glaciers, are not even included. Nevertheless, our results strongly support long-term scaling at least for 200 years. Further, the comparison between control run and historical

Table 1. Continental Average α Values and Corresponding Standard Deviations for Eurasia, Africa, America, and Australia, Obtained From the Historical Simulation and the Control Run, Both in Daily and Biannual Resolution[a]

	Daily Data		Biannual Data	
Continent	Historical Simulation	Control Run	Historical Simulation	Control Run
Eurasia	0.62 ± 0.04	0.60 ± 0.04	0.67 ± 0.06	0.61 ± 0.06
Africa	0.61 ± 0.04	0.55 ± 0.05	0.68 ± 0.06	0.57 ± 0.07
North America	0.60 ± 0.05	0.59 ± 0.07	0.66 ± 0.06	0.63 ± 0.10
Australia	0.55 ± 0.06	0.52 ± 0.04	0.62 ± 0.07	0.54 ± 0.07

[a]Compare to Figure 2. We would like to remark that this averaging to some extent masks the results for very continental sites, since there are more land grid points with maritime climate. We use the following areas (top left to bottom right): Eurasia, (−7.50°E, 79.78°N)–(−176.25°E, 38.97°N), (52.50°E, 35.26°N)–(120.00°E, 9.28°N); Africa, (−15.00°E, 35.26°N)–(48.75°E, −31.54°N); America, (−165.00°E, 83.48°N)–(−56.25°E, 12.99°N), (−82.50°E, 9.28°N)–(−37.50°E, −50.10°N); and Australia, (116.25°E, −5.57°N)–(150.00°E, −38.97°N).

simulation shows, that the forcings are essential for the long-term correlations in the temperature records.

[38] We could verify neither the claim that the long-term correlations vanish in the middle of the continents [*Fraedrich and Blender*, 2003; see also *Bunde et al.*, 2004] nor that the strength of these correlations increases from the poles to the equator [*Huybers and Curry*, 2006]. Both claims not only differ from our findings for the model runs, but are also in remarkable contrast to the enormous number of observational data [*Eichner et al.*, 2003; *Király et al.*, 2006]. Since in particular the results of *Huybers and Curry* [2006] are opposite to our results, we would like to comment on them in more detail. *Huybers and Curry* [2006] use Thomson's multitaper method to characterize the surface air temperatures from the NCEP-NCAR model (instrumental reanalysis 1948–2002). In their Figure 1.d the authors plot versus the latitude the spectral exponents $\beta = 2\alpha - 1$ [see, e.g., *Kantelhardt et al.*, 2001], determined on scales between 2 months and 30 years after removing the annual oscillations and harmonics. For ocean grid points, *Huybers and Curry* [2006] report $\beta > 1$ ($\alpha > 1$) at the equator and $\beta \approx 0$ ($\alpha \approx 0.5$) at the poles. The reason for the contradiction in the results of *Huybers and Curry* [2006] and this work, are probably due the different model, different method, and different timescales. In addition, the authors find anticorrelations between the annual cycle and the long-term correlations: the weaker the annual cylce, the stronger the long-term correlations. On the basis of proxy and some instrumental records, *Huybers and Curry* [2006] quantify in their Figure 2 on scales between 1.1 and 100 years $\beta = 0.37...0.56$ ($\alpha = 0.69...0.78$) and on scales between 100 and 15,000 years they find $\beta = 1.29...1.64$ ($\alpha \approx 1.15...1.32$). We like to note that latter are also considerably larger than those we obtained recently for several reconstructed temperatures of the Northern Hemisphere [*Rybski et al.*, 2006], ranging up to 2000 years.

[39] Finally, in this paper, we only studied temperature records and focused exclusively on the linear correlation properties. It is an interesting question how far the global climate models are able to reproduce also the nonlinear "multifractal" features of the climate system [see *Koscielny-Bunde et al.*, 1998; *Weber and Talkner*, 2001; *Govindan et al.*, 2003; *Ashkenazy et al.*, 2005; *Bartos and Jánosi*, 2006; *Livina et al.*, 2007]. It is known that in particular rainfall is significantly multifractal [see, e.g., *Tessier et al.*, 1996; *Kantelhardt et al.*, 2006], and it will be interesting to see if this feature is also reflected in model rain fall data.

[40] **Acknowledgments.** We would like to thank the German Federal Ministry of Education and Research for financial support. We are particularly grateful to Sebastian Wagner for indispensable help, especially in handling the data, and we would like to thank Eduardo Zorita and Jan F. Eichner for useful discussions.

References

Ashkenazy, Y., D. R. Baker, and H. Gildor (2005), Simple stochastic models for glacial dynamics, *J. Geophys. Res.*, *110*, C02005, doi:10.1029/2004JC002548.

Bartos, I., and I. M. Jánosi (2006), Nonlinear correlations of daily temperature records over land, *Nonlinear Processes Geophys.*, *13*(5), 571–576.

Bunde, A., S. Havlin, J. W. Kantelhardt, T. Penzel, J.-H. Peter, and K. Voigt (2000), Correlated and uncorrelated regions in heart-rate fluctuations during sleep, *Phys. Rev. Lett.*, *85*(17), 3736–3739.

Bunde, A., S. Havlin, E. Koscielny-Bunde, and H.-J. Schellnhuber (2002), Atmospheric Persistence Analysis: Novel Approaches and Applications, in *The Science of Disasters*, chap. 5, pp. 171–191, Springer, Berlin.

Bunde, A., J. F. Eichner, S. Havlin, E. Koscielny-Bunde, H.-J. Schellnhuber, and D. Vyushin (2004), Comment on "Scaling of Atmosphere and Ocean Temperature Correlations in Observations and Climate Models,", *Phys. Rev. Lett.*, *92*(3), 039801.

Chen, Z., P. C. Ivanov, K. Hu, and H. E. Stanley (2002), Effect of nonstationarities on detrended fluctuation analysis, *Phys. Rev. E*, *65*(4), 041107.

Crowley, T. J. (2000), Causes of climate change over the past 1000 years, *Science*, *289*, 270–277.

Eichner, J. F., E. Koscielny-Bunde, A. Bunde, S. Havlin, and H.-J. Schellnhuber (2003), Power-law persistence and trends in the atmosphere: A detailed study of long temperature records, *Phys. Rev. E*, *68*(4), 046133.

Etheridge, D. M., L. P. Steele, R. L. Langenfelds, R. J. Francey, J. M. Barnola, and V. I. Morgan (1996), Natural and anthropogenic changes in atmospheric CO_2 over the last 1000 years from air in antarctic ice and firn, *J. Geophys. Res.*, *101*(D2), 4115–4128.

Fraedrich, K., and R. Blender (2003), Scaling of atmosphere and ocean temperature correlations in observations and climate models, *Phys. Rev. Lett.*, *90*(10), 108501.

Glantz, M. H. (2000), *Currents of Change—Impacts of El Niño and La Niña on Climate and Society*, Cambridge Univ. Press, Cambridge, U. K.

Govindan, R. B., D. Vyushin, A. Bunde, S. Brenner, S. Havlin, and H.-J. Schellnhuber (2002), Global climate models violate scaling of the observed atmospheric variability, *Phys. Rev. Lett.*, *89*(2), 028501.

Govindan, R. B., A. Bunde, and S. Havlin (2003), Volatility in atmospheric temperature variability, *Physica A*, *308*, 529–536.

Huybers, P., and W. Curry (2006), Links between annual, Milankovitch and continuum temperature variability, *Nature*, *441*(7091), 329–332.

Kantelhardt, J. W., E. Koscielny-Bunde, H. H.A. Rego, S. Havlin, and A. Bunde (2001), Detecting long-range correlations with detrended fluctuation analysis, *Physica A*, *295*, 441–454.

Kantelhardt, J. W., E. Koscielny-Bunde, D. Rybski, P. Braun, A. Bunde, and S. Havlin (2006), Long-term persistence and multifractality of precipitation and river runoff records, *J. Geophys. Res.*, *111*, D01106, doi:10.1029/2005JD005881.

Kaplan, A., M. A. Cane, Y. Kushnir, A. C. Clement, M. B. Blumenthal, and B. Rajagopalan (1998), Analyses of global sea surface temperature 1856–1991, *J. Geophys. Res.*, *103*(C9), 18,567–18,589.

Király, A., I. Bartos, and I. M. Jánosi (2006), Correlation properties of daily temperature anomalies over land, *Tellus, Ser. A*, *58*(5), 593–600.

Koscielny-Bunde, E., A. Bunde, S. Havlin, and Y. Goldreich (1996), Analysis of daily temperature fluctuations, *Physica A*, *231*, 393–396.

Koscielny-Bunde, E., A. Bunde, S. Havlin, H. E. Roman, Y. Goldreich, and H.-J. Schellnhuber (1998), Indication of a universal persistence law governing atmospheric variability, *Phys. Rev. Lett.*, *81*(3), 729–732.

Koutsoyiannis, D. (2006), Nonstationarity versus scaling in hydrology, *J. Hydrol.*, *324*(1–4), 239–254.

Lean, J., J. Beer, and R. Bradley (1995), Reconstruction of solar irradiance since 1610: Implications for climate change, *Geophys. Res. Lett.*, *22*(23), 3195–3198.

Legutke, S., and R. Voss (1999), The Hamburg atmosphere-ocean coupled model ECHO-G, *Tech. Rep. 18*, German Comput. Cent. for Clim. Res. (DKRZ), Hamburg, Germany.

Livina, V., Z. Kizner, P. Braun, T. Molnar, A. Bunde, and S. Havlin (2007), Temporal scaling comparison of real hydrological data and model runoff records, *J. Hydrol.*, *336*(1–2), 186–198.

Mandelbrot, B. B., and J. R. Wallis (1968), Noah, Joseph, and operational hydrology, *Water Resour. Res.*, *4*(5), 909–918.

Monetti, R. A., S. Havlin, and A. Bunde (2003), Long-term persistence in the sea surface temperature fluctuations, *Physica A*, *320*, 581–589.

Pelletier, J. D., and D. L. Turcotte (1997), Long-range persistence in climatological and hydrological time series: analysis, modeling and application to drought hazard assessment, *J. Hydrol.*, *203*(1–4), 198–208.

Peng, C.-K., S. V. Buldyrev, S. Havlin, M. Simons, H. E. Stanley, and A. L. Goldberger (1994), Mosaic organization of DNA nucleotides, *Phys. Rev. E*, *49*(2), 1685–1689.

Roeckner, E., et al. (1996), The atmospheric general circulation model ECHAM-4: Model description and simulation of present-day climate, *Tech. Rep. 218*, Max Planck Inst. für Meteorol., Hamburg, Germany.

Rybski, D., A. Bunde, S. Havlin, and H. von Storch (2006), Long-term persistence in climate and the detection problem, *Geophys. Res. Lett.*, *33*, L06718, doi:10.1029/2005GL025591.

Talkner, P., and R. O. Weber (2000), Power spectrum and detrended fluctuation analysis: Application to daily temperatures, *Phys. Rev. E*, *62*(1), 150–160.

Tessier, Y., S. Lovejoy, P. Hubert, D. Schertzer, and S. Pecknold (1996), Multifractal analysis and modeling of rainfall and river flows and scaling, causal transfer functions, *J. Geophys. Res.*, *101*(D21), 26,427–26,440.

Vyushin, D., I. Zhidkov, S. Havlin, A. Bunde, and S. Brenner (2004), Volcanic forcing improves Atmosphere-Ocean Coupled General Circulation Model scaling performance, *Geophys. Res. Lett.*, *31*(10), L10206, doi:10.1029/2004GL019499.

Weber, R. O., and P. Talkner (2001), Spectra and correlations of climate data from days to decades, *J. Geophys. Res.*, *106*(D17), 20,131–20,144.

Wolff, J. O., E. Maier-Reimer, and S. Legutke (1997), The Hamburg Primitive Equation Model HOPE, *Tech. Rep. 18*, German Comput. Cent. for Clim. Res. (DKRZ), Hamburg, Germany.

Zorita, E., F. González-Rouco, and S. Legutke (2003), Testing the Mann et al. (1998) approach to paleoclimate reconstructions in the context of a 1000-yr control simulation with the echo-g coupled climate model, *J. Clim.*, *16*(9), 1378–1390.

Zorita, E., J. F. González-Rouco, H. von Storch, J. P. Montávez, and F. Valero (2005), Natural and anthropogenic modes of surface temperature variations in the last thousand years, *Geophys. Res. Lett.*, *32*(8), L08707, doi:10.1029/2004GL021563.

A. Bunde and D. Rybski, Institut für Theoretische Physik III, Universität Giessen, D-35392 Giessen, Germany. (armin.bunde@theo.physik.uni-giessen.de)

H. von Storch, Institute for Coastal Research, GKSS Research Centre, D-21502 Geesthacht, Germany.